20th International Conference on
Harmonisation within Atmospheric Dispersion Modelling for Regulatory Purposes
14-18 June 2021, Tartu, Estonia

THE ROLE OF THERMAL CONVECTION IN THE DISPERSION OF TRAFFIC-INDUCED AIR POLLUTANTS IN THE URBAN ENVIRONMENT

Bálint Papp [1] *and Gergely Kristóf* [1]

[1] Budapest University of Technology and Economics, Faculty of Mechanical Engineering, Department of Fluid Mechanics (H-1111, Budapest, Műegyetem rkp. 3.)

Abstract: In the present study, the combined effect of natural wind and thermal convection is analyzed using a Finite Volume Method based CFD solver utilizing Large Eddy Simulation. By assuming a periodically repeated building pattern as a simplistic representation of the city, the size of the computational domain – thus the computational demand – is substantially reduced, and by applying the previously developed Transient Wind Forcing method, the effect of large-scale turbulence, causing extensive changes in wind direction and magnitude, is captured. Thermal effects and buoyancy are also taken into account in the periodic space under the assumption of constant wall temperatures. Based on the transient periodic flow field, the plume emitted from a point source can be reconstructed at any time instance based on the individual particle trajectories. The effect of the Richardson number ($Ri = Gr\,Re^{-2}$) on the flow structures and the dispersion processes is investigated, and requirements for comparable field experiments are formulated.

Keywords: *street canyon, thermal convection, periodic geometry, Large Eddy Simulation (LES), Lagrangian particle tracking, Transient Wind Forcing (TWF)*

1. INTRODUCTION

Pedestrian exposure to traffic-induced air pollutants is critical in calm wind conditions when the ventilation of the urban canopy is dominated by local convection. The most current investigations include non-isothermal field experiments (**Chen et al., 2020**), wind tunnel measurements (**Allegrini, 2018**; **Lin et al., 2020**; **Chen et al., 2021**), as well as CFD simulations (**Chew et al., 2018**; **Hang et al., 2020**). The urban canopy in these analyses is often modeled by repetitive building patterns, including high-rise buildings or street canyons, with heated ground and/or walls. The literature on non-isothermal street canyons is recently reviewed by **Zhao et al. (2020).** Most studies agree that the flow and dispersion phenomena depend on the bulk Richardson number (Ri), characterizing the ratio of buoyancy and inertial forces:

$$Ri = \frac{Gr}{Re^2} = \frac{gL\beta(T_{wall} - T_0)}{U_{ref}^2} \tag{1}$$

In the above expression, Gr [–] is the Grashof number, and Re [–] is the Reynolds number, in which g [kg m s^{-2}] denotes the gravitational acceleration, L [m] is the characteristic size, in our case, the roof height H, $\beta = T_0^{-1}$ [K^{-1}] is the thermal expansion coefficient, T_{wall} [K] and T_0 [K] are the temperatures of the heated surfaces and the bulk flow, respectively, and U_{ref} [m s^{-1}] is the characteristic velocity.

2. THE APPLIED CFD MODEL

2.1. Geometry, mesh, boundary conditions

In the present study, as a simplistic model of the city, an infinite series of infinitely long street canyons of uniform, $H/W = 2$ aspect ratio was investigated. The dimensions of the computational domain were $X \times Y \times Z = 1.1$ m $\times$ 1.1 m $\times$ 3.6 m, with the building height being $H = 1.2$ m (**Figure 1a**). An equidistant hexahedral mesh of $W/32$ resolution was created, with inflations in the vicinity of the walls. Periodic boundary conditions were applied in the x and y directions at all horizontal boundaries, and symmetry was assumed at the top of the domain. Representing the heating of the walls by the sunlight, the top and the windward face of the buildings were assigned a constant temperature (T_{wall} = 303 or 333 K in different cases, designated by red lines), while the rest of the solid surfaces were adiabatic. Additionally, an

isothermal reference case was run with no wall heating. The initial temperature of air was $T_0 = 293$ K. The propulsion for imposing the natural wind (**Figure 1b**) is described in **Section 2.2.**

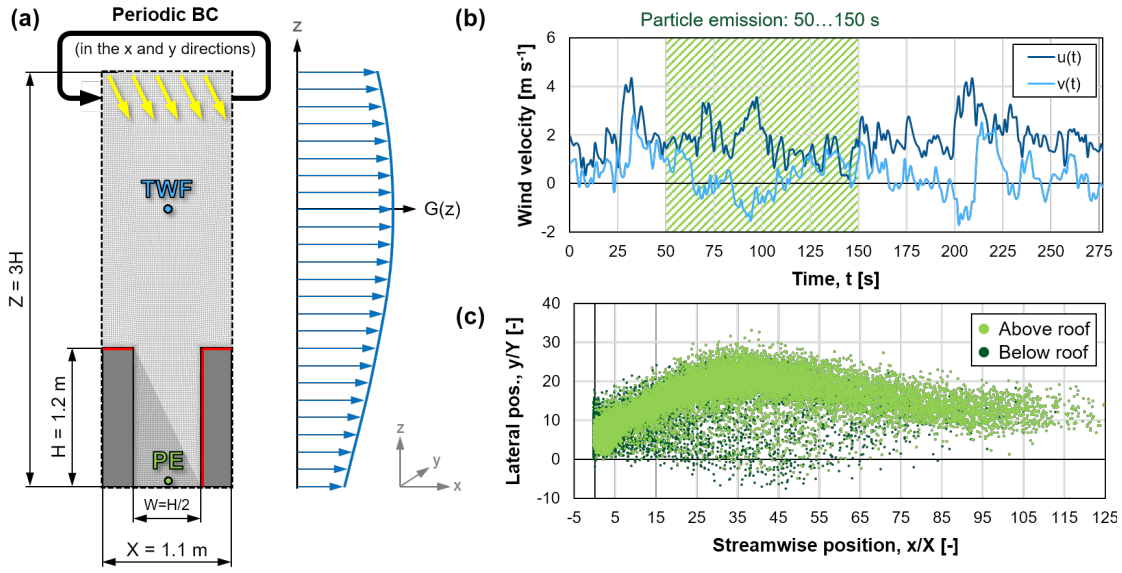

Figure 1. (a) Dimensions of the simulation domain (lateral size: $Y = 1.1$ m), mesh, and boundary conditions. (b) Measured velocity time series used for propulsion (source: **Kristóf et al., 2020**). (c) Bird's eye view of the particles over the first 125 street canyons at $t = 150$ s for $Ri = 0.47$ (with $\Delta T = 40$ K). Particles are released at the origin.

2.2. Velocity control and turbulence modeling

In periodic models, symmetry condition is commonly used at the upper boundary, so it is necessary to compensate for the surface drag with a distributed driving force. Most LES models use a homogeneous body force corresponding to a constant pressure gradient, which also determines the direction and magnitude of the average wind speed. According to the Transient Wind Forcing model (**Kristóf et al. 2020**), the direction and magnitude of the transient driving force are determined by controlling the velocity at an observation point based on measured velocity-time series (**Figure 1b**). The relaxation time of the velocity control is determined based on the largest turbulent length scale resolved in the model, so the effect of *macroscopic turbulence* (flow structures larger than the domain size) can be taken into account by the relatively slowly varying driving force. The TWF method utilizes horizontally homogenous and vertically inhomogeneous volume sources of momentum ($G(z)$ distribution in **Figure 1a**) in both x and y directions (S_u and S_v, respectively). The formula for the x component of the driving force is given in **Equation (2)**.

$$S_u(z,t) = \rho_0 \cdot \frac{u_m(t) - u(t)}{\tau(t)} \cdot e^{-\frac{1}{2}\left(\frac{z-z_0}{L_0}\right)^2} \tag{2}$$

In the expression for S_u [N m^{-3}], ρ_0 [kg m^{-3}] is the air density, u_m [m s^{-1}] and u [m s^{-1}] denote the measured and computed x-direction velocity components at time t [s], and τ [s] is the relaxation time of the velocity control, which is initialized with the simulation time step and relaxed to the resolution of the reference time series (1 s). The vertical force distribution is Gaussian, in which z [m] is the vertical coordinate, $z_0 = 2H$ is the center of the propulsion (i.e., the measurement height), and $L_0 = X = Y$ is the radius of the propulsion profile. The formulation of S_v based on the v velocity components is similar to **Equation (2).** For modeling *mesoscopic (resolved) turbulence*, i.e., flow structures between the domain size and the grid resolution, Large Eddy Simulation was applied, and *microscopic (sub-grid scale) turbulence* was taken into account by the Smagorinsky-Lilly model (with $C_s = 0.1$). The constant time step size was set to satisfy the CFL condition.

2.3. Temperature control

In the lower part of the atmospheric boundary layer corresponding to our model range, we can assume that the sensible heat fluxes are approximately in equilibrium: the heat transferred from the building surfaces to

the air flow is balanced by the turbulent heat flux at the top of the investigated zone; thus the average air temperature is approximately constant. In the periodic model, the constant average air temperature is provided by a volume source of heat according to **Equation (3)**. This relationship is, in fact, a generalization of the heat source for a channel with translational periodicity, derived by **Patankar et al. (1977)**, to bi-directional (*x, y*) periodicity, in which the dominant wind can take any horizontal directions ($\overrightarrow{d_0}$).

$$S_T(\vec{x},\, t) = -\rho_0 c_v \cdot \frac{T_{avg}(t) - T_0}{\Delta x} \cdot \left[\vec{v}(\vec{x},\, t) \cdot \overrightarrow{d_0}\right] \tag{3}$$

In the above equation, S_T [W m^{-3}] is a volumetric heat source, c_v [J kg^{-1} K^{-1}] is the specific heat of air at constant volume, T_{avg} [K] is the current volume average temperature of air, T_0 [K] is a pre-defined reference temperature (initial average temperature), and Δx [m] is the mesh resolution. Moreover, $\vec{v}(\vec{x},\, t)$ [m/s] denotes the velocity field, and $\overrightarrow{d_0}$ [–] is the unit vector designating the mean wind direction. In our experience, using the mesh resolution in the above formula results in a sufficiently fast and also numerically stable control term (i.e., the temperature difference $T_{avg} - T_0$ does not exceed 0.1 K throughout the entire simulation). Note that, as an option, the velocity-weighted bulk temperature (T_{bulk}) and the current velocity vector ($\vec{d}$) could have also been used in the place of T_{avg} and $\overrightarrow{d_0}$.

2.4. Dispersion model

The original TWF model (**Kristóf et al., 2020**) is already capable of tracking particles even outside of the boundaries of the periodic domain by counting how many times each particle jumped a in either direction due to the periodic BCs. In other words, despite having only one canyon in the model, even the far-field dispersion of various sources can be calculated. Furthermore, **Papp et al. (2021)** demonstrated that the mean concentration field can also be accurately calculated based on the Lagrangian particle model.

$$c^* = \frac{dU_{ref}A}{t_s/\Delta t} = \frac{dU_{ref}A}{N_p} \tag{4}$$

In the above formula for the mean normalized concentration, $c^*(x, y, z)$ [–], d [s m^{-3}] is the dose, calculated based on the total residence time of the particles in each cell per cell volume, $U_{ref} = 1.87$ [m s^{-1}] is the mean wind velocity magnitude, $A = XY = 1.21$ (m^2) is the plan area of the periodic raster, $t_s = 100$ (s) is the length of the emission (from 50 s to 150 s in all cases, see **Figure 1b**), and Δt [s] is the time step size. For a continuous particle emission at a single point (location: $x_{PE}/H = y_{PE}/H = 0$, $z_{PE}/H = 0.05$, see **Figure 1a**), the total particle count is $N_p = t_s/\Delta t$. The ventilation efficiency is evaluated by using the mass Stanton number (the dimensionless mass transfer coefficient), which can be obtained as the reciprocal of the near-ground ($z/H < 0.1$) average concentration in all canyons.

$$k^* = \frac{1}{c^*_{ng}} \tag{5}$$

3. RESULTS AND DISCUSSION

In the present study, seven cases of the same geometry are demonstrated in the range of $Re = U_{ref}H/\nu = 15\,300 \ldots 153\,000$ and $Ri = 0.47 \ldots 47$, with an additional isothermal baseline case ($Re = 153\,000$, $Ri = 0$). These conditions were achieved by re-scaling the original time series (**Figure 1b**) by 0.1…1 and applying $\Delta T = 0$, 10, and 40 K temperature differences. The characteristic vertical profiles obtained by averaging between 50…277 s of flow time (0…50 s: flow conditioning) and in $\Delta z/H = 20$ thick horizontal layers are shown in **Figure 2**, along with the ventilation coefficient as the function of *Ri*.

The velocity distribution in the boundary layer over the canopy depends on the Richardson number; however, we observed a significant Reynolds number dependence of the flow within the $H/W = 2$ street canyon in the isothermal cases in the $Re = 15\,300 \ldots 76\,300$ range, similarly to the findings of **He et al. (2017)**. Moreover, in the presence of heated windward walls, vertical flows due to thermal convection introduce additional turbulence within and above the canopy, which phenomenon is more pronounced for the high *Ri* cases; hence, in non-isothermal cases a larger velocity jump can be observed at roof height, compared to the $Ri = 0$ case. It can also be observed that the normalized temperature profiles cover wider ranges for lower *Ri*.

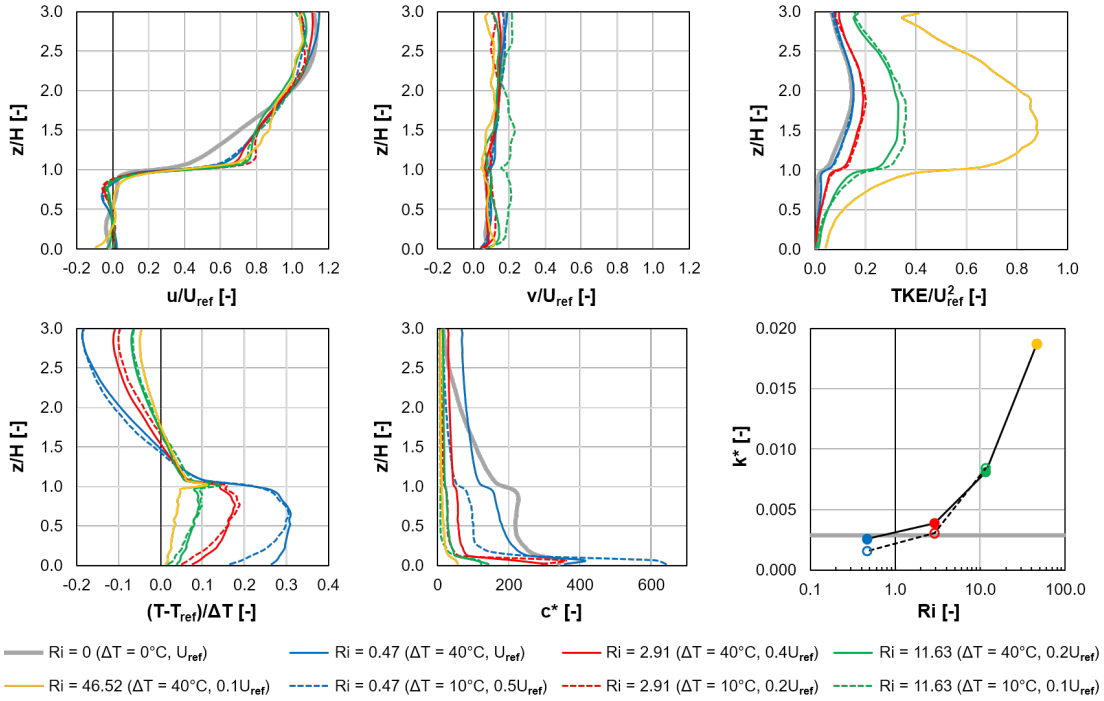

Figure 2. Vertical profiles of the normalized u and v velocity components, resolved turbulence kinetic energy, temperature, and total concentration, along with the ventilation efficiencies (k*) at various Richardson numbers.

It can be concluded based on the normalized concentration diagrams, and the ventilation coefficients plotted in **Figure 2** that heating the windward walls of $H/W = 2$ street canyons hinders the canyon vortex, thus decreasing pollutant removal at low Ri. On the other hand, at moderately high Richardson numbers, the ventilation of the urban canopy is indeed improved. Another interesting phenomenon, also observed by **Xie et al. (2005)** for $H/W = 1$ street canyons, is shown in **Figure 3:** even for low (non-zero) Ri, a secondary counter-rotating vortex develops at the bottom of the canyon; thus, the traffic-induced air pollutants accumulate near the windward (downstream) wall, contrary to the isothermal case ($Ri = 0$) when particles escape the canyon close to the leeward (upstream) wall.

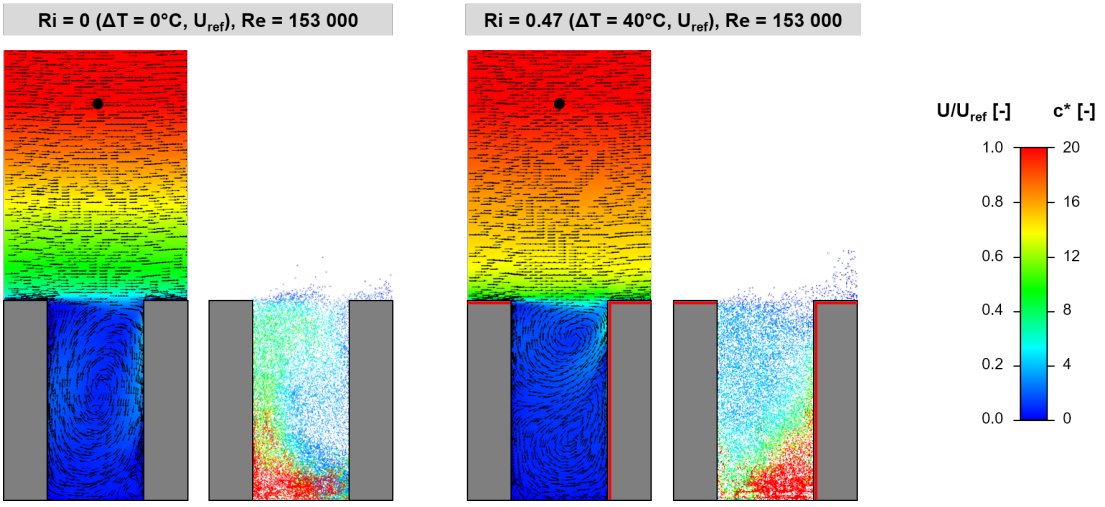

Figure 3. Flow visualization for an isothermal (left) and a heated (right) case of the same Reynolds number. Contour plots and vectors of the normalized mean velocity magnitude in a cut plane at $y = 0$. Instantaneous particle clouds in the first canyon at $t = 150$ s (at the end of the emission), colored by the local time-averaged concentration.

4. CONCLUSIONS AND OUTLOOK

In this paper, a proof of concept was demonstrated for a measurement-based transient simulation method, including the effects of natural convection using a periodic domain. Model validation requires further efforts. Requirements for the measurement data and the benefits of the present CFD model are listed below.

4.1. Requirements for measurement data to be comparable with the presented CFD results

- Periodic or quasi-periodic geometry.
- Time series of two horizontal velocity components at a reference location and further gauging points.
- The temporal resolution of the velocity time series is at least 1 Hz for full-scale experiments. (This frequency limit decreases for small-scale geometries, according to the model scale.)
- The measurement covers at least 500-1000 flow-through times for stable concentration results.
- The measurement includes either steady or time-dependent ambient and wall temperatures.
- The measurement may include mean and time-dependent concentration results as well.

4.2. Thermal Transient Wind Forcing (T-TWF) model features

- The effects of natural wind – such as sudden changes in direction and magnitude – are taken into account using Large Eddy Simulation. Even the effects of flow structures exceeding the domain size can be modeled in a relatively small periodic domain using TWF. (Validation: **Kristóf et al., 2020**.)
- Based on the periodic flow field, time-dependent particle tracks exceeding the domain boundaries can be calculated, and long-distance dispersion can also be modeled. (Validation: **Papp et al., 2021**.)
- The effects of buoyancy and natural convection can be taken into account in the fully periodic space.

REFERENCES

Allegrini, J. (2018). *A wind tunnel study on three-dimensional buoyant flows in street canyons with different roof shapes and building lengths.* **Building and Environment, 143,** 71-88.

Chen, G., Wang, D., Wang, Q., Li, Y., Wang, X., Hang, J., Gao, P., Ou, C., &Wang, K. (2020). *Scaled outdoor experimental studies of urban thermal environment in street canyon models with various aspect ratios and thermal storage.* **Science of The Total Environment, 726,** 138147.

Chen, L., Hang, J., Chen, G., Liu, S., Lin, Y., Mattsson, M., ... & Ling, H. (2021). *Numerical investigations of wind and thermal environment in 2D scaled street canyons with various aspect ratios and solar wall heating.* **Building and Environment, 190**, 107525.

Chew, L. W., Glicksman, L. R., & Norford, L. K. (2018). *Buoyant flows in street canyons: Comparison of RANS and LES at reduced and full scales.* **Building and Environment, 146**, 77-87.

Hang, J., Chen, X., Chen, G., Chen, T., Lin, Y., Luo, Z., ... & Wang, Q. (2020). *The influence of aspect ratios and wall heating conditions on flow and passive pollutant exposure in 2D typical street canyons.* **Building and Environment, 168**, 106536.

He, L., Hang, J., Wang, X., Lin, B., Li, X., & Lan, G. (2017). *Numerical investigations of flow and passive pollutant exposure in high-rise deep street canyons with various street aspect ratios and viaduct settings.* **Science of the Total Environment, 584**, 189-206.

Kristóf, G., Papp, B., Wang, H., & Hang, J. (2020). *Investigation of the flow and dispersion characteristics of repeated orographic structures by assuming transient wind forcing.* **Journal of Wind Engineering and Industrial Aerodynamics, 197,** 104087.

Lin, Y., Ichinose, T., Yamao, Y., & Mouri, H. (2020). *Wind velocity and temperature fields under different surface heating conditions in a street canyon in wind tunnel experiments.* **Building and Environment, 168**, 106500.

Papp, B., Kristóf, G., Istók, B., Koren, M., Balczó, M., & Balogh, M. (2021). *Measurement-driven Large Eddy Simulation of dispersion in street canyons of variable building height.* **Journal of Wind Engineering and Industrial Aerodynamics, 211,** 104495.

Patankar, S. V., Liu, C. H., & Sparrow, E. M. (1977). *Fully developed flow and heat transfer in ducts having streamwise-periodic variations of cross-sectional area.* **Journal of Heat Transfer, 99 (2)**

Xie, X., Huang, Z., Wang, J., & Xie, Z. (2005). *The impact of solar radiation and street layout on pollutant dispersion in street canyon.* **Building and Environment, 40(2)**, 201-212.

Zhao, Y., Chew, L. W., Kubilay, A., & Carmeliet, J. (2020). Isothermal and non-isothermal flow in street canyons: A review from theoretical, experimental and numerical perspectives. **Building and Environment, 184**, 107163.